physica status solidi

pss

www.pss-journals.com

reprint

WILEY-VCH

Phys. Status Solidi B **250**, No. 10, 2085–2089 (2013) / **DOI** 10.1002/pssb.201384228

physica status solidi b
www.pss-b.com
basic solid state physics

Graphene nanofilm as pressure and force sensor: A mechanical analysis

K. Kam[1], F. Scarpa[*,1], S. Adhikari[2], and R. Chowdhury[3]

[1] Advanced Composites Centre for Innovation and Science, University of Bristol, BS8 1TR Bristol, UK
[2] Multidisciplinary Nanotechnology Centre, Swansea University, SA2 8PP Swansea, UK
[3] Department of Civil Engineering, Indian Institute of Technology Roorkee, Roorkee, Uttarakhand, India

Received 23 September 2011, revised 14 July 2012, accepted 3 August 2013
Published online 2 October 2013

Keywords graphene, mass sensor, nonlinear loading

[*] Corresponding author: e-mail f.scarpa@bristol.ac.uk Phone: +44 117 315306, Fax: +44 117 9272771

The out-of-plane mechanical bending properties of single layer graphene sheets (SLGS) are modelled using a molecular mechanics approach based on an atomistic–finite element formulation. Force/displacement curves for different rectangular SLGS with different aspect ratios are obtained for distributed (uniform pressure) and concentrated central loadings. We show that membrane and bending deformations scale differently based on the type of load, as well as geometry of the graphene sensor films.

1 Introduction During the last decade, the discovery of superlattice monolayers [1] and thin films in graphite (i.e. 'graphene' [2]) has led to the development of novel devices for nanoelectronics [3], nano strain gages [4] and electrodes for innovative nanocircuits [5]. Particular attention has been devoted to the possible use of single layer graphene as mass sensors and resonators [6, 7]. The nonlinear mechanical behaviour of graphene sheets subjected to central point loading has been studied analytically by Hemmasizadeh et al. [8], and verified experimentally by Lee et al. [9] on circular graphene sheets. Another possible mechanical loading effect is given by distributed uniform pressure, which may arise either by confinement of the graphene in modern non-functionalized nanocomposites [10], or by the presence of molecules in proximity of the graphene layer [11]. While the out-of-plane behaviour under concentrated loading has been evaluated using semi-analytical [8] and atomistic–continuum approaches [12] for circular graphene sheets, less attention has been devoted to rectangular graphene films, with the exception of wrinkling effects due to boundary effects under nanondentation [13]. To the best of our knowledge, however, no analysis has been carried out on the mechanical performance of rectangular graphene sheets under distributed loading. In this work, we use an atomistic–finite element (FE) approach to model the nonlinear out-of-plane mechanical behaviour of rectangular graphene sheets with different aspect ratios subjected to both central and distributed loading. The atomistic–FE approach used in this work has been used to simulate the mechanical properties of carbon nanotubes [14, 15], single [16] and bilayer graphene [17]. A peculiarity of this modelling approach consists in identifying the distribution of average equilibrium lengths of the sp^2 bonds, as well as the value of the thickness of the nanostructure minimising the total potential energy of the system, resolving therefore the so-called 'Yakobson's paradox' [18], and an enhanced identification of the engineering constants of the nanomaterial. The force (or pressure)/displacement relations for rectangular single layer graphene sheets (SLGS) will be derived, and compared against analogous results from equivalent continuum isotropic material plates subjected to the same type of loading. We will show that graphene behaves in a significant different way from a transverse isotropic material in out-of-plane deformations, and that the mechanical response of the nanofilms is significantly dependent over the type of loading applied.

2 The model The total steric potential of the sp^2 C–C bonds can be represented in the following form [19]:

$$U_{\text{total}} = U_r + U_\theta + U_\tau, \tag{1}$$

where U_r is the bond stretching energy, U_θ is bond angle variation and U_τ is the combined dihedral angle and out-of-plane torsion. Equation (1) ignores the electrostatic and van der Waal's forces as they are not the main contributors to the total steric potential in covalent systems for linear elastic deformations [20]. More specifically, these terms can be expressed as [20]:

$$U_r = \frac{1}{2} k_r (\delta r)^2 , \tag{2}$$

$$U_\theta = \frac{1}{2} k_\theta (\delta\theta)^2 , \tag{3}$$

$$U_\tau = \frac{1}{2} k_\tau (\delta\phi)^2 , \tag{4}$$

where k_r, k_θ and k_τ are force constants related to bond stretching, bending and torsional stiffness. δr, $\delta\theta$ and $\delta\phi$ are the variations in bond stretch, in-plane and twisting angle increments. Following Scarpa et al. [16], we assume that the C–C bonds behave as beams with uniform circular cross section (the thickness d), with stretching, bending, torsion and deep-shear deformation of their cross section. The strain energies for axial and torsion loading, together with the combined in-plane bending/shear deformation can be expressed and equated to the steric potential as:

$$\begin{aligned} \frac{k_r}{2} (\delta r)^2 &= \frac{EA}{2L} (\delta r)^2 , \\ \frac{k_\tau}{2} (\delta\phi)^2 &= \frac{GJ}{2L} (\delta\phi)^2 , \\ \frac{k_\theta}{2} (\delta\theta)^2 &= \frac{EI}{2L} \frac{4+\Phi}{1+\Phi} (\delta\theta)^2 . \end{aligned} \tag{5}$$

In (5), L is the length of the equivalent beam representing the C–C bond, A the cross section of the beam, I and J the moment and polar moment of inertia respectively. The first row of (5) is related to the equivalence between stretching and axial deformation mechanism (with E being the equivalent Young's modulus), while the second one equates the torsional deformation of the C–C bond with the pure shear deflection of the structural beam associated to an equivalent shear modulus G. Contrary with similar approaches previously used [20, 21], the term equating the in-plane rotation of the C–C bond (third row of 5) is equated to a bending strain energy related to a deep shear beam model, to take into account the shear deformation of the cross section. The shear correction term becomes necessary when considering beams with aspect ratio lower than 10 [22]. For circular cross sections, the shear deformation constant can be expressed as [16]:

$$\Phi = \frac{12EI}{GA_s L^2} . \tag{6}$$

In (6), $A_s = A/F_s$ is the reduced cross section of the beam by the shear correction term F_s depending on the Poisson's ratio ν of the equivalent material [23]:

$$F_s = \frac{6 + 12\nu + 6\nu^2}{7 + 12\nu + 4\nu^2} . \tag{7}$$

The insertion of (6) and (7) in (5) leads to an nonlinear relation between the thickness d and the Poisson's ratio ν of the equivalent beam [16]:

$$k_\theta = \frac{k_r d^2}{16} \frac{4\Omega + B}{\Omega + B} , \tag{8}$$

where

$$\Omega = 112L^2 k_\tau + 192L^2 k_\tau \nu + 64L^2 k_\tau \nu^2 , \tag{9}$$

$$B = 9k_r d^2 + 18k_r d^4 \nu + 9k_r d^4 \nu^2 . \tag{10}$$

The values for the force constants for the AMBER and linearized Morse potential models can be found in Table 1. The equivalent mechanical properties of the C–C bond can be determined performing a nonlinear optimization of (5) using a Marquardt algorithm, obtaining a functional relation between the thickness d and the equivalent Poisson's ratio of the C–C bond ν. The C–C bond itself can then be discretized as a single two-nodes three-dimensional FE model beam with a 6×6 stiffness matrix $[\mathbf{K}]_e$ described in Ref. [24], where the nodes represent the atoms. For nonlinear geometric loading, a secant stiffness matrix is obtained following the standard procedures of FE [25].

Table 1 Force constant values for AMBER and linearized Morse potential.

potential	k_r (N nm^{-1})	k_θ (N nm rad^{-2})	k_τ (N nm rad^{-2})
AMBER	6.52×10^{-7}	8.76×10^{-10}	2.78×10^{-10}
Morse potential	8.74×10^{-7}	9.00×10^{-10}	2.78×10^{-10}

The SLGSs are assembled as planar truss-type plates in graphitic state (i.e. with the location of the carbon atoms lying in a single plane – see Fig. 1). Although this geometric assumption is a simplification of the real equilibrium

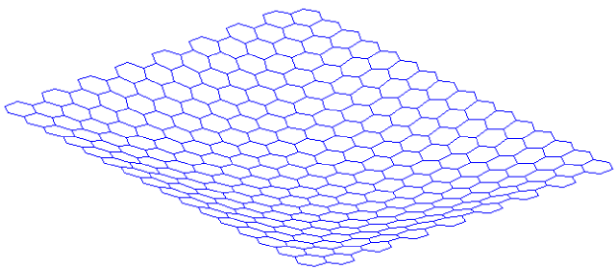

Figure 1 Rectangular SLGS under uniform pressure distribution (3.86 nm × 3.31 nm).

configuration of SLGSs observed from MD and DFT simulations, nonetheless it provides a satisfying approximation of the overall homogenized mechanical properties in sp^2-based systems [4, 8, 26]. The plates are fully clamped on their edges, and subjected to a uniform pressure distribution q across their overall surface, or central point loading $F = q\,b^2$, where b is the side lengths of the graphene sheets. A nonlinear geometric static loading analysis is carried out using a Newton–Raphson solver with 30 substeps [12]. During the post-processing of the results, the total potential energy of the system is calculated and considered as the objective function of a two-steps nonlinear minimization process made of a zero order and first order solver [12]. The variables of the minimization procedure are the thickness d, equivalent Poisson's ratio of the sp^2 bond material ν and average equilibrium length of the C–C bonds L, the latter describing the uneven distribution of the sp^2 bond lengths arising due to the boundary conditions, chirality and mechanical loading in graphene systems [27, 28]. The admissible values for of the thickness vary in a range of $0.69 < d < 0.87$ Å for the linearized Morse potential [16]; the average equilibrium length is $0.135 < L < 0.142$ nm, consistently with the values identified by Reddy et al. [28] using Cauchy–Borne rule. The Poisson's ratio of the hypothetical equivalent material for the sp^2 bond assumes a range of $-1.0 < \nu < 0.5$, reflecting a homogeneous isotropic material.

3 Results and discussion The minimization of the total potential energy leads to the identification of the thickness d and average length L. From these quantities, it is possible to infer the tensile rigidity Y_1, Poisson's ratio ν_{12} and shear modulus G_{12} of the graphene plate considering the linear elastic deformations of the SLGS in graphitic state are governed by stretching–hinging mechanism [16, 29]:

$$Y_1 = \frac{4\sqrt{3}k_r K_h}{3(k_r + 3K_h)}, \tag{11}$$

$$\nu_{12} = \frac{1 - K_h/k_r}{1 + 3K_h/k_r}, \tag{12}$$

$$G_{12} = \frac{\sqrt{3}k_r K_h}{3d(k_r + K_h)}. \tag{13}$$

For the specific calculation of the hinging constant K_h the Reader can consult Refs. [15, 16]. The tensile rigidity calculated using the atomistic–continuum approach of Eqs. (11) and (12) for uniaxial tensile loading (see Ref. [16]) is equal to 0.297 and 0.384 TPa nm for the AMBER and Morse potential force models respectively, while Poisson's ratio is 0.211 and 0.213 [16]. The linearized Morse potential force model shares a closer tensile rigidity with the majority of the other models available in open literature (see Table 2), and has been therefore adopted for all the force/pressure-deflection simulations.

Table 3 shows the numerical results for the SLGS Young's and shear modulus, and Poisson's ratios obtained from Eqs. (11)–(13) from the energy-minimized values of d. The symbols a and b stand for the dimensions of the rectangular nanofilm. The results are related to both point and distributed loading. The tensile rigidity shows good agreement with 0.329 TPa nm for the smallest rectangular graphene sheet from Scarpa et al. [12]. The average equilibrium bond length identified is 0.135 nm, similar to bond lengths observed by Reddy et al. [28] in SLGSs with uniaxial and bi-axial loading. The Young and shear moduli remain constant for different aspect ratios at 3.84 and 1.45 TPa, respectively. Similarly, the thickness remains constant at 0.87 Å, giving a tensile rigidity of 0.334 TPa nm for all aspect ratios and loading. The high value of the thickness in bending (0.87 Å against the 0.79 Å identified for in-plane loading [16]) suggests that the sp^2 C–C bond behaves similarly to an hyper-elastic (rubber-like) material, with an equivalent Poisson's ratio $\nu = 0.46$. The graphene layers under bending behave as homogenized isotropic materials, with $G_{12} \approx E_1/2(1 + \nu_{12})$ for all load cases and aspect ratios. These models show remarkable similarities in terms of tensile rigidity and thickness compared to Kudin et al. [30] from *ab initio* computations (0.345 TPa nm and 0.89 Å), but their model has a lower Poisson's ratio (0.149).

Scarpa et al. [12] modified Hemmasizadeh et al. [8] formulation for point loading graphene, and obtained a relationship between the nondimensional out-of-plane force

Table 2 Tensile rigidity and Poisson's ratio values for graphene in open literature.

author	Y_{SLGS} (TPa nm)	ν_{SLGS}	d (Å)
Scarpa et al. (AMBER) [16]	0.297	0.211	0.84
Scarpa et al. (Morse) [16]	0.384	0.213	0.74
Scarpa et al. (FE Morse [16]), and Tu and Ou-Yang [32]	0.353	0.34	0.75
Lier et al. [33]	0.377	N/A	3.4
Kudin et al. [30]	0.345	0.149	0.89
Li and Chou [34]	0.349	N/A	3.4
Tserpes and Papanikos [20]	0.351	N/A	1.47
Huang et al. [35]	0.243	0.397	0.57

Table 3 Graphene out-of-plane bending results for both load cases for Young's modulus and Poisson's ratio, averaged over different pressures.

aspect ratio	a (nm)	b (nm)	E_1 (TPa)	G_{12} (TPa)	ν_{12}	Y_1 (TPa nm)	d (Å)
distributed loading							
1.17	3.86	3.31	3.84	1.45	0.32	0.33	0.87
2.29	3.86	1.69	3.84	1.45	0.32	0.33	0.87
4.40	3.86	0.88	3.84	1.45	0.32	0.33	0.87
point loading							
1.17	3.86	3.31	3.84	1.45	0.32	0.33	0.87
2.29	3.86	1.69	3.84	1.45	0.32	0.33	0.87
4.40	3.86	0.88	3.84	1.45	0.32	0.33	0.87

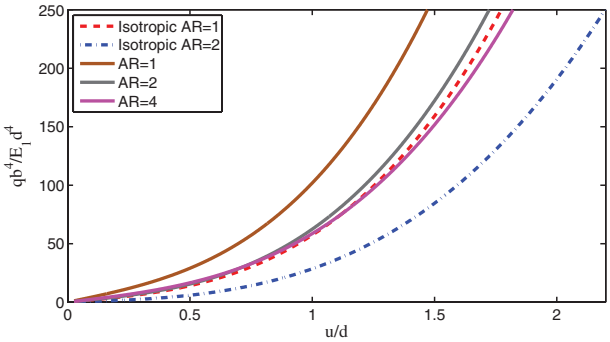

Figure 2 Nondimensional force–displacement curves for uniform pressure distribution q.

against nondimensional deflection:

$$\frac{qb^4}{E_1 d^4} = \frac{K_1}{1-\nu_{12}^2}\left(\frac{u}{d}\right) + K_2\left(\frac{u}{d}\right)^3, \tag{14}$$

where q is the pressure on the graphene sheet, u is the out-of-plane bending deflection and K_1 and K_2 are constants dependent on the aspect ratio of the graphene sheet. The Young's modulus E_1 is defined as Y_1/d. Equation (14) neglects the effects from pre-stress obtained through mechanical or thermal loading. Figures 2 and 3 show the nondimensional forces against nondimensional deflection for the distributed and point loads, fitted against Equation (14). For the distributed pressure case, Fig. 2 shows also the comparison against analytical formulas related to plates subjected to the same loading, but composed by a classical isotropic material [31]. The graphs shows a nonlinear $(u/d)^3$ dependent on the flexural deformation of the graphene, while the membrane stress dictates the (u/d) term. The out-of-plane stiffness dependence over the cube of the deformation has been also observed experimentally by Lee et al. [9] using an AFM to indent graphene suspended over trenches with circular holes. It is worth noticing that the experimental value of the tensile rigidity from Ref. [9] (0.340 TPa nm), is only 2.6% higher than the one predicted by our model. The rectangular graphene sheets show a higher sensitivity to out-of-plane deflection when subjected to a concentrated point load. This

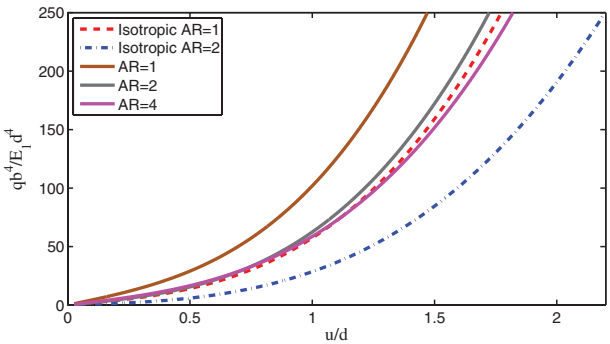

Figure 3 Nondimensional force–displacement curves for central point loading $F = q\,b^2$.

Table 4 K_1 and K_2 for different aspect ratios and load cases for a Poisson's ratio of 0.32.

aspect ratio	K_1	K_2	R^2
pressure loading			
1.17	38.9	58.5	1.00
2.29	18.4	41.9	0.99
4.40	22.1	34.0	0.99
point loading			
1.17	13.7	6.0	0.99
2.29	7.9	2.0	0.99
4.40	6.5	0.7	0.99
square plate with equivalent isotropic material [31]			
pressure loading	16.5	38.9	0.99
point loading	5.6	22.2	0.99

fact can be explained using also 2D beam theory [31]. Consider a elastic cantilever beam subjected to distributed and point load, which have maximum deflections respectively equal to $w_a l^4/8EI$ and $Wl^3/3EI$, where w_a is load per unit span, while W is the point load. When $w_a = W/l$, the point load has a larger maximum deflection at the tip than distributed load by a factor 2.67.

Table 4 shows the K_1 and K_2 coefficients of Eq. (14) for different aspect ratios of the graphene sheets for $\nu_{12} = 0.32$. The R^2 correlation between Eq. (14) and the nonlinear force/deflection curves obtained by the atomistic–FE models shows a good fit for all the aspect ratios considered. For the case of pressure loading, the graphene sheets results show a similar trend as the isotropic thin plate , where K_1 is smaller than K_2. In square aspect ratios (1.17 in our case), the ratio K_2/K_1 is close to 1.5, significantly lower than the 2.54 for a classical isotropic material plate. This fact suggests that out-of-plane membrane deformations in graphene scale higher than the bending ones. For higher aspect ratios, the increased importance of membrane stresses is more pronounced, although for aspect ratios higher than for K_2/K_1 is close to 1.5, as for the square plate. Point loading follows the opposite trend, showing a lower K_2 than K_1, similarly to what observed for circular graphene sheets [12]. For all the aspect ratios considered, the membranal stiffness is considerably higher compared to the isotropic material plate case (2.42 times the increase of K_1 for the almost square aspect ratio). The nondimensional bending stiffness, on the other hand, is decreased as much as 31 times (K_2 term), when compared to a plate made with a classical continuum isotropic material. The peculiar departures from the isotropic continuum plate representation can be ascribed to the effective in-plane orthotropy of the finite size graphene sheets [16, 19, 28], as well as the edge effects in rectangular graphene [12]. When comparing K_1 and K_2 between point loading and distributed loading for aspect ratio of 1.17, a decrease of 64.9% and 89.7% can be seen. A larger decrease in K_2 suggests that membrane-induced deformations dominate in point loading models. As

the aspect ratio increases, both K terms are decreasing, with the exception of the distributed cases with aspect ratios of 2.29 and 4.40.

4 Conclusions We have shown the force/displacement relations of graphene nanofilms subjected to both uniform pressure distribution and concentrated point loading, obtained through an atomistic–FE approach. The model used allows to identify a set of equivalent thickness and bending stiffness very close to values present in open literature, both based on molecular models and experimental results. The nondimensional force/displacement relations highlight the peculiar mechanical behaviour of single layer finite size graphene sheets, where the edge effects play a significant role in the overall equivalent out-of-plane mechanical behaviour. Moreover, the results highlight the fact that the equivalent mechanical continuum behaviour of nanomaterials can be described adequately when the nano-entities are considered as *structures*. Their mechanical response and overall behaviour will therefore depend on the geometry, temperature and loading conditions. The nondimensional force/displacements equations could be used to design and predict the behaviour of mass sensors subjected to nonlinear loading.

References

[1] Y. Gan, W. Chu, and L. Qiao, Surf. Sci. **539**(1–3), 120–128 (2003).
[2] A. K. Geim and K. S. Novoselov, Nature Mater. **6**(3), 183–191 (2007).
[3] V. Barone, O. Hod, and G. V. Scuseria, Nano Lett. **6**(12), 2748 (2006).
[4] A. Sakhaee-Pour, M. T. Ahmadian, and A. Vafai, Solid State Commun. **147**(7–8), 336–340 (2008).
[5] K. S. Kim, Y. Zhao, H. Jang, S. Y. Lee, J. M. Kim, K. S. Kim, J.-H. Ahn, P. Kim, J.-Y. Choi, and B. H. Hong, Nature **457**(7230), 706–710 (2009).
[6] C. Chen, S. Rosenblatt, K. I. Bolotin, W. Kalb, P. Kim, I. Kymissis, H. L. Stormer, T. F. Heinz, and J. Hone, Nature Nanomater. **4**, 861–867 (2009).
[7] C. L. Wong, M. Annamalai, Z. Q. Wang, and M. Palaniapan, J. Micromech. Microeng. **20**, 115029 (2010).
[8] A. Hemmasizadeh, M. Mahzoon, and E. Hadi, Thin Solids Films **416**, 7636 (2008).
[9] C. Lee, X. Wei, J. W. Kysar, and J. Hone, Science **321**(5887), 385–388 (2008).
[10] J. Cho, J. J. Luo, and I. M. Daniel, Compos. Sci. Technol. **67**, 2399 (2007).
[11] K. Jensen, K. Kim, and A. Zettl, Nature Nanomater. **3**, 533–537 (2008).
[12] F. Scarpa, S. Adhikari, A. J. Gil, and C. Remillat, Nanotechnology **21**(12), 125702 (2010).
[13] A. J. Gil, S. Adhikari, F. Scarpa, and J. Bonet, J. Phys.: Condens. Matter **22**, 145302 (2010).
[14] F. Scarpa and S. Adhikari, J. Phys. D, Appl. Phys. **41**(8), 085306 (2008).
[15] F. Scarpa, L. Boldrin, H. X. Peng, C. D. L. Remillat, and S. Adhikari, Appl. Phys. Lett. **97**(15), 151903 (2010).
[16] F. Scarpa, S. Adhikari, and A. S. Phani, Nanotechnology **20**, 065709 (2009).
[17] F. Scarpa, S. Adhikari, and R. Chowdhury, Phys. Lett. A **374**(19–20), 2053–2057 (2010).
[18] O. A. Shenderova, V. V. Zhirnov, and D. W. Brenner, Crit. Rev. Solid State Mater. Sci. **27**, 227 (2002).
[19] C. D. Reddy, S. Rajendran, and K. M. Liew, Int. J. Nanosci. **4**(4), 631 (2005).
[20] K. I. Tserpes and P. Papanikos, Composites B **36**, 468 (2005).
[21] A. Sakhaee-Pour, M. T. Ahmadian, and R. Naghdabadi, Nanotechnology **19**, 085702 (2008).
[22] S. Timoshenko, Theory of Plates and Shells (McGraw-Hill, Inc., London, 1940).
[23] T. Kaneko, J. Phys. D, Appl. Phys. **8**, 1927 (1974).
[24] J. S. Przemienicki, Theory of Matrix Structural Analysis (McGraw-Hill, New York, 1968).
[25] O. Zienkiewicz, The Finite Element Method (McGraw-Hill, Inc., London, 1977).
[26] A. Sakhaee-Pour, Solid State Commun. **149**(1–2), 91 (2009).
[27] S. Rajendran and C. D. Reddy, J. Comput. Theor. Nanosci. **3**, 1 (2006).
[28] C. D. Reddy, S. Rajendran, and K. M. Liew, Nanotechnology **17**, 864 (2006).
[29] P. P. Gillis, Carbon **22**(4–5), 387 (1984).
[30] K. N. Kudin, G. E. Scuseria, and B. I. Yakobson, Phys. Rev. B **64**, 235406 (2001).
[31] W. C. Young and R. G. Budynas, Roark's Formulas for Stresses and Strains, seventh ed. (McGraw-Hill, Inc., London, 2002).
[32] Z. Tu and Z. Ou-Yang, Phys. Rev. B **65**, 233407 (2002).
[33] G. V. Lier, C. V. Alsenoy, V. V. Doren, and P. Greelings, Chem. Phys. Lett. **326**, 181 (2000).
[34] C. Li and T. W. Chou, Phys. Rev. B **68**, 073405 (2003).
[35] Y. Huang, J. Wu, and K. C. Hwang, Phys. Rev. B **74**, 245413 (2006).